

Analysis of the SIMPLE Pressure-Correction Algorithm for Lid-Driven Cavity Flow

Numerical Modelling for Incompressible Flows Assignment

MSc CFD



Adam James Brierley, 458865
Prepared for MONDAY, 3RD MARCH, 2025

Contents

1 INTRODUCTION	2
2 LITERATURE REVIEW	2
3 INCOMPRESSIBLE METHODOLOGY	5
3.1 Governing Equations	5
3.2 Solution Approaches	6
3.3 The SIMPLE Algorithm	7
3.4 The Algorithm	9
3.5 The 2-D Lid-driven Cavity	10
4 RESULTS AND DISCUSSION	11
5 Conclusions and Future Work	16
References	17

1 INTRODUCTION

Cavity flows are used frequently as a benchmark problem in the research setting, with many different iterations on the simple 2D case, to investigate quite fundamental questions about fluid mechanics[1]. The SIMPLE method, a pressure-correction type method developed by Patankar and Spalding in 1972, is used extensively in industry as a robust method[2]. The purpose of this report is to verify and validate an implementation of the SIMPLE method, and analyse it's effectiveness against this well-studied benchmark.

The state-of-the-art now for lid-driven cavity flow research is high Reynolds numbers, turbulence, 3D cavities, non-Newtonian fluids, multiple moving walls, or variations in geometry, as a brief overview. Advances in computing power have enabled tremendously complex problems to be investigated, such as the corner flows of a 3D cavity. They also appear in industrial applications such as short-dwell coaters and melt spinning processes used to manufacture micro-crystalline material[3]. In addition, the eddy structures in cavity flow can inform us of behaviour for applications like drag-reducing riblets and mixing cavities, used to synthesise fine polymeric composites[4]. Within the research setting, their use is as a benchmark problem to investigate many types of fluid phenomena and as a test case for developments in numerical methods. Given that the simple geometry and boundary conditions are combined with a fluid flow system that includes almost all fluid phenomena of special interest, such as eddies, secondary flows, complex 3D phenomena, chaotic particle motions, instabilities, transition and turbulence, it is an ideal case study. Importantly, it's simplicity and easy adoption allow extensive comparison amongst researchers and engineers, and all the while fundamental problems remain unanswered. It is for these reasons that the flows should be understood and investigated.

2 LITERATURE REVIEW

Good review papers in lid-driven cavity flow are provided by Shankar and Deshpande, who wrote in the early 2000s, as well as Kuhlmann and Romano, who wrote more recently in 2019[4][1]. The earliest numerical solution to 2D lid-driven cavity was by Kawaguti for the Physical Society of Japan in 1961, who used the streamfunction-vorticity formulation[5]. His results are presented in figure 1. Importantly, he only achieved accurate results up to a Reynolds number of 64, divergence occurring at $Re = 128$. Furthermore, in this early study secondary flow was not observed in the corners. Figure 1c shows the main recirculating eddy, which spans the entire channel, migrates towards the downstream corner with increasing Reynolds number.

This was followed soon after with investigations by Burggraf, who's primary focus was the viscous structure of the recirculating eddy[6]. A linearised analytical solution was compared with the numerical solution which uses a relaxation procedure. Burggraf highlights that as the Reynolds number is increased a finer lattice is required, owing to the decreasing thickness of the viscous layer. In the regime investigated by Kawaguti (0 to 64), Burggraf points out that viscous effects permeate the entire flow field and that as Reynolds number is increased an eddy with an inviscid rotational core develops, as predicted by Batchelor[7]. At lower Reynolds numbers, the vortex core shifts away from the centre, and as the inviscid core develops above around $Re = 100$, it begins to shift back. This is because inertial effects begin to dominate at higher Reynolds numbers. Unlike Kawaguti, Burggraf finds the secondary flows in the corner regions are present for all Reynolds numbers. The importance of pressure gradient in the formation of secondary corner regions is also commented on, which may have particular implications for the SIMPLE method. From $Re = 0, 100, 400$, Burggraf highlights that the streamlines remain topologically similar, and that it's vorticity plots which provide a stronger measure of viscosity.

A seminal paper regarding lid-driven cavity flow came 20 years later from Ghia *et al.*[8], who use the vorticity-streamfunction formulation with multigrid methods to investigate square lid-driven cavity flow up to a much higher

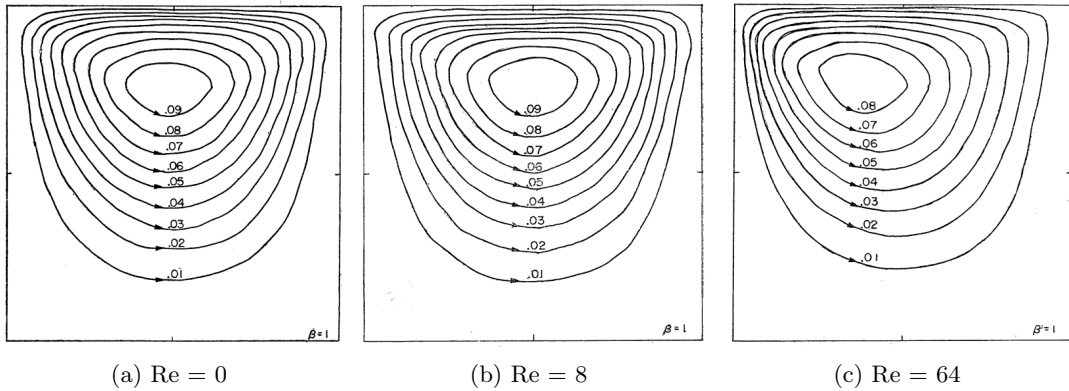
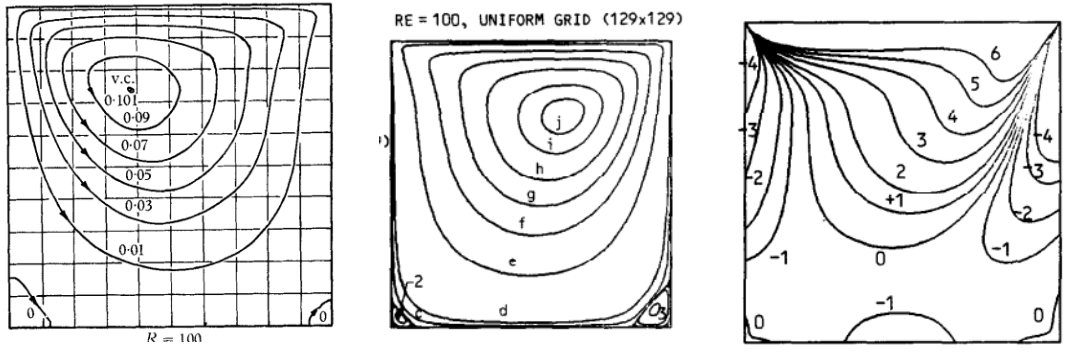


Figure 1: Streamlines of Kawaguti[5]. Flow is from right to left.



(a) Burggraff streamlines for $Re = 100$. (b) Ghia streamlines for $Re = 100$. (c) Ghia vorticity for $Re = 100$.

Reynolds number, $Re = 10,000$. It is notable how the growth in computing power facilitated approach to higher Reynolds numbers. This was on a 129×129 and 257×257 grid, the higher Re requiring finer grids. Initially, $Re = 100$ is used to validate the method given the abundance of data for this specification. We compare with these results in this paper. Ghia comments on the thinning of the wall boundary layers as Reynolds number is increased, as evident in the centreline velocity profiles[8]. It is observed that the near-linearity of the velocity profiles in the centre of the cavity is evidence of uniform vorticity which develops here for larger Re . For high Re , a kink is observed in the velocity profiles near the top of the cavity. Given that this kink persists with the finer mesh, Ghia suggests the velocity distribution near the wall is less sensitive to mesh size than ϕ and ω at the vortex centre, for example. Ghia *et al.* results are given in figure 2b and 2c and are used for the purposes of comparison with results

The review paper by Kuhlmann and Romano is more recent and provides some newer insights since Ghia *et al.*[1]. As already mentioned Ghia *et al.* but also Schreiber and Keller extended the study to $Re = 10,000$ and improved on the accuracy and efficiency of Kawaguti and Burggraf[9]. Koseff and Street then carried out experiments on 3D cavities[10]. A new level of accuracy for 2D was supposedly reached by Botella and Peyret, who used spectral methods

and a direct treatment of the singular corners[11]. Kuhlmann comments that the singular corners may effect numerical accuracy.

The corner discontinuities are a special case of Taylor's scraping problem and require special analytical and numerical treatment, because vorticity and pressure diverge[15]. This may effect numerical accuracy. This is also a difficult issue in experiment because of the gap, which can lead to leaking or pumping. The other interesting phenomena is the appearance of infinite self-similar vortices in the lower corners, predicted by Moffat, whose size and intensity decay in geometric progression[14].The Batchelor theorem, that in 2D steady lid-driven cavity flow, in the absence of instabilities, a vortex with an inviscid core of uniform velocity surrounded by viscous boundary layers appears, was proved experimentally and numerically. It also became clearer over time that the 2D steady flow was not stable at higher Reynolds numbers. Hopf bifurcations have been shown to occur in 2D cavities at around $Re = 8000$, though there is poor agreement for the critical Reynolds number amongst researchers. In the current report, the flow remains steady.

3 INCOMPRESSIBLE METHODOLOGY

3.1 Governing Equations

In reality, all fluid flows are compressible to a small degree, and liquids are significantly less compressible than gases. For incompressible flows, the primary assumption is that the density will not vary. This is indeed true for low Mach numbers, that is roughly $M < 0.2$ or $M < 0.3$. Consider the continuity equation,

$$\frac{\partial \rho}{\partial t} + \nabla \cdot (\rho \mathbf{u}) \equiv \frac{\partial \rho}{\partial t} + \text{div}(\rho \mathbf{u}) = 0 \quad (1)$$

which represents the fundamental law of nature which is conservation of mass.

We can expand the second term which is divergence of momentum using the product rule,

$$\frac{\partial \rho}{\partial t} + \rho \cdot (\nabla \cdot \mathbf{u}) + \mathbf{u} \cdot \nabla \rho \equiv \frac{\partial \rho}{\partial t} + \rho \cdot \text{div} \mathbf{u} + \mathbf{u} \cdot \text{grad} \rho = 0 \quad (2)$$

We now use our primary assumption, which is that density of the fluid medium is constant, and thus the first and third terms in equation 2 disappear,

$$\rho \cdot (\nabla \cdot \mathbf{u}) \equiv \rho \cdot \text{div} \mathbf{u} = 0 \quad (3)$$

And dividing by the constant, density,

$$\boxed{\nabla \cdot \mathbf{u} = 0} \quad (4)$$

This is the **divergence-free velocity constraint** or the **incompressibility constraint**. It can be demanding for the incompressible solver to satisfy. Indeed, the performance of the solver can be judged by how well it meets this constraint. In reality, divergence of velocity is roughly 10e-6 to 10e-9 in most fluid media; most solvers might accomplish 10e-2 or 10e-1. Physically, this equation implies that there is no volumetric expansion or contraction in control volumes of the fluid media.

The difficulty that arises for incompressible flows is that there is no independent equation for the pressure field. The equation of state is no longer valid, so that,

$$p \neq \rho \cdot R \cdot T \quad (5)$$

$$p \neq p(\rho) \quad (6)$$

$$\rho \neq \rho(p) \quad (7)$$

Approaches to this problem will be returned to later.

Consider the **compressible** Navier-Stokes equations with Gibbs' and Hamilton's vector notation and the non-linear convective/advection term in conservative form,

$$\frac{\partial(\rho \mathbf{u})}{\partial t} + \nabla \cdot (\rho \mathbf{u} \otimes \mathbf{u}) = \rho \cdot \mathbf{g} - \nabla p + \mu \nabla^2 \mathbf{u} + \frac{\mu}{3} \nabla (\nabla \cdot \mathbf{u}) \quad (8)$$

Remove the final term using the divergence-free velocity constraint (equation 4) and divide by the density for the incompressible Navier-Stokes equation,

$$\frac{\partial \mathbf{u}}{\partial t} + \nabla \cdot (\mathbf{u} \otimes \mathbf{u}) = \mathbf{g} - \frac{1}{\rho} \nabla p + \frac{\mu}{\rho} \nabla^2 \mathbf{u} \quad (9)$$

With the non-linear term in a non-conservative form, the **incompressible** Navier-Stokes momentum equation is,

$$\boxed{\frac{\partial \mathbf{u}}{\partial t} + (\mathbf{u} \cdot \nabla) \mathbf{u} = \mathbf{g} - \frac{1}{\rho} \nabla p + \frac{\mu}{\rho} \nabla^2 \mathbf{u}} \quad (10)$$

The left hand side represents the contributions to the velocity of the fluid particle, a local acceleration and non-linear (self-feeding) convective component. In the manner of Newton's second law, these accelerations are balanced by forces on the right hand side, which are the pressure fields and viscosity fields. The third term on the RHS is the diffusion of momentum due to the viscosity. For example, in 2-D cavity flow the no-slip condition of the moving lid means adjacent fluid parcels match its velocity, and the viscosity diffuses this velocity or momentum to other adjacent fluid parcels, whilst also dissipating energy via shear stress. That is, shear stresses diffuse momentum and in the process generate heat (dissipation). The final term in equation 8 is shear stress from volumetric expansion or contraction, which here is neglected. The gravity (body) force is also neglected. The density is constant for the whole field, so it is not a dependent variable. Hence, we have a relationship between accelerations and forces.

Thus together equation 4 and equation 10 represent the physics of our incompressible fluid flow. Boundary conditions and initial conditions specify our problem, as well as an approach for coupling the pressure and velocity field, because there is no independent equation for the pressure field. In particular, the requirement is to have a meaningful, physically correct mathematical expression for the pressure field. Over the years several incompressible flow strategies and solvers have been developed which are summarised below,

3.2 Solution Approaches

- I . Pressure-Poisson approach of Harlow & Welch (1951).
- II . Artificial compressibility method of Chorin (1967).
- III . Pressure-projection method of Chorin (1968).
- IV . Vector potential - vorticity formulation.
- V . FSAC-PP.
- VI . Pressure-Correction methods.

3.3 The SIMPLE Algorithm

In 1972 Patankar and Spalding introduced the Semi-Implicit Method for Pressure-Linked Equations (SIMPLE)[2]. This deals with the problem of the unknown pressure field since the equation of state is now invalid. As mentioned in Patankar's textbook, 'Numerical Heat Transfer and Fluid Flow', the pressure field is specified indirectly via the continuity equation[12]. If the correct pressure field is substituted, the velocity field will satisfy the continuity equation. This forms the basis of the method.

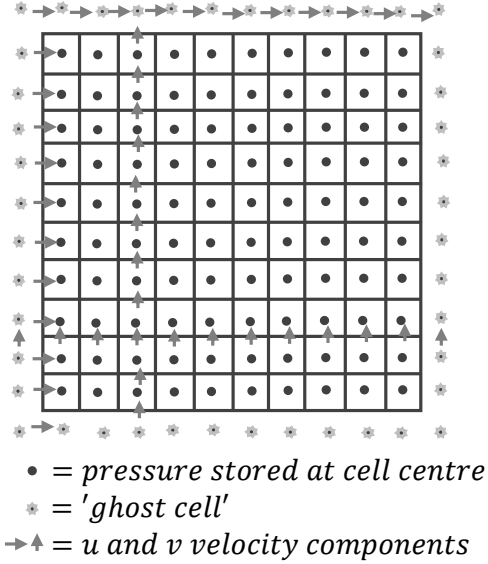


Figure 3: Staggered grid of Harlow and Welch used to discretise the computational domain[13].

In discretising the pressure gradient term in equation 10, the potential for a wavy or oscillatory field to not be accounted when integrating over the control volume arises, with the so-called 'zigzag' or 'checkerboard' effect. A highly non-uniform pressure field could be missed. This is because the discretised form of the pressure gradient term depends only on neighbouring values (it should be highlighted that a piecewise-linear distribution or interpolation of the dependent variable is assumed in this procedure).

Harlow and Welch at Los Alamos introduced a remedy in 1965 along with their 'Marker and Cell' or 'MAC' method, which was to stagger the grid for different variables[13]. This meant separate or offset control volumes were treated for u, v, and p respectively. This arrangement as implemented in this report is shown in figure 3. This prevents the checkerboard effect. There are some questions as to whether the method is still necessary given the high grid resolution facilitated by modern computing power. The method does add extra interpolations and storage for indexing. for example.

The following discretisation is used for the momentum equations,

$$a_e u_e = \Sigma a_{nb} u_{nb} + b + (p_P - p_E) A_e \quad (11)$$

where the last term is the force on the volume due to the pressure field, and a_{nb} represents the combined convection-diffusion influence at the control volume faces. The momentum equations discretised here can only be solved if the pressure field is known. We guess a pressure field p^* , which gives imperfect velocity fields u^*, v^* (which do not satisfy continuity),

$$a_e u_e^* = \Sigma a_{nb} u_{nb}^* + b + (p_P^* - p_E^*) A_e \quad (12)$$

$$a_n w_n^* = \Sigma a_{nb} v_{nb}^* + b + (p_P^* - p_N^*) A_n \quad (13)$$

The guessed pressure field is then corrected,

$$p = p^* + p' \quad (14)$$

The velocity components respond,

$$u = u^* + u' \quad (15)$$

$$v = v^* + v' \quad (16)$$

Subtract equation 12 from 11 to get the correction,

$$a_e u'_e = \Sigma a_{nb} u'_{nb} + (p'_P - p'_E) A_e \quad (17)$$

Drop the $\Sigma a_{nb} u'_{nb}$ term.

$$a_e u'_e = (p'_P - p'_E) A_e \quad (18)$$

Divide by a_e ,

$$u'_e = d_e (p'_P - p'_E) \quad (19)$$

$$d_e \equiv \frac{A_e}{a_e} \quad (20)$$

The **velocity-correction formulae**,

$$\boxed{u_e = u_e^* + d_e (p'_P - p'_E)} \quad (21)$$

This shows how u_e^* is to be corrected in response to the corrected pressure field to produce u_e . The continuity equation is then used to find the pressure-correction equation which is not shown here but the reader is referred to Patankar's textbook[2]. Here the b term represents a mass source to be annihilated to satisfy continuity.

$$\boxed{v_n = v_n^* + d_n (p'_P - p'_N)} \quad (22)$$

3.4 The Algorithm

Thus, the algorithm is carried out as follows,

- Guess the pressure field p^* .
- Obtain the imperfect velocity fields, u^*, v^* , by solving the discretised momentum equations (11) with p^* substituted.
- Obtain an equation for the velocity corrections, u', v' , using equation 17, eliminate terms.
- Obtain u, v as in equation 21.
- Substitute u, v to find the pressure-correction equation, p' , using a coefficients and annihilate b , the mass source term.
- Calculate p by adding p' to p^* .
- Treat corrected p as the new p^* .

3.5 The 2-D Lid-driven Cavity

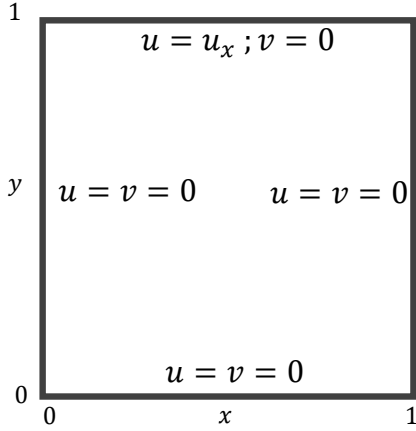


Figure 4: Computational Domain.

By assuming the width of a 3-D cavity extends to infinity, or is at least very long, we can assume the flow is 2-D. Three dimensional effects are therefore negligible. Studying 2D flows is useful in general and especially where the width is large. Three dimensional lid-driven cavity flow is much more complex, with problems such as dealing with the lower corner regions in 3D only having been approached recently.

New boundary conditions are imposed in the Fortran code by altering the a coefficients. There are no-slip boundary conditions on all walls as well as impermeability applied. The lid has horizontal velocity $u = 1$, that is from left to right. So-called 'ghost cells' or image cells are used, as shown in figure 3, to apply the boundary conditions. Simulation parameters and fluid properties used are displayed in tables 1 and 2.

Convergence Criteria	Max. Its	P Underrelaxation	U Underrelaxation	V Underrelaxation	Scalar Underrelaxation
1.e-6	5000	0.6	0.6	0.6	1.0

Table 1: Simulation Parameters.

Density ($\frac{kg}{m^3}$)	Dynamic Viscosity ($\frac{kg}{m \cdot s}$)	Peclet
998.2	0.00103	10

Table 2: Fluid Parameters.

4 RESULTS AND DISCUSSION

Figure 5 shows how the flowfield is organised through the cavity for a Reynolds number of 100 and a 129x129 grid. The influence each term of the governing equation has on the fluid is considered. The explicit form is repeated here for convenience,

$$\frac{\partial \mathbf{u}(x, y, t)}{\partial t} + (\mathbf{u}(x, y, t) \cdot \nabla) \mathbf{u}(x, y, t) = -\frac{1}{\rho} \nabla p(x, y, t) + \frac{\mu}{\rho} \nabla^2 \mathbf{u}(x, y, t) \quad (23)$$

where the continuity equation is used to indirectly get the pressure field by annihilating mass sources and applying pressure corrections.

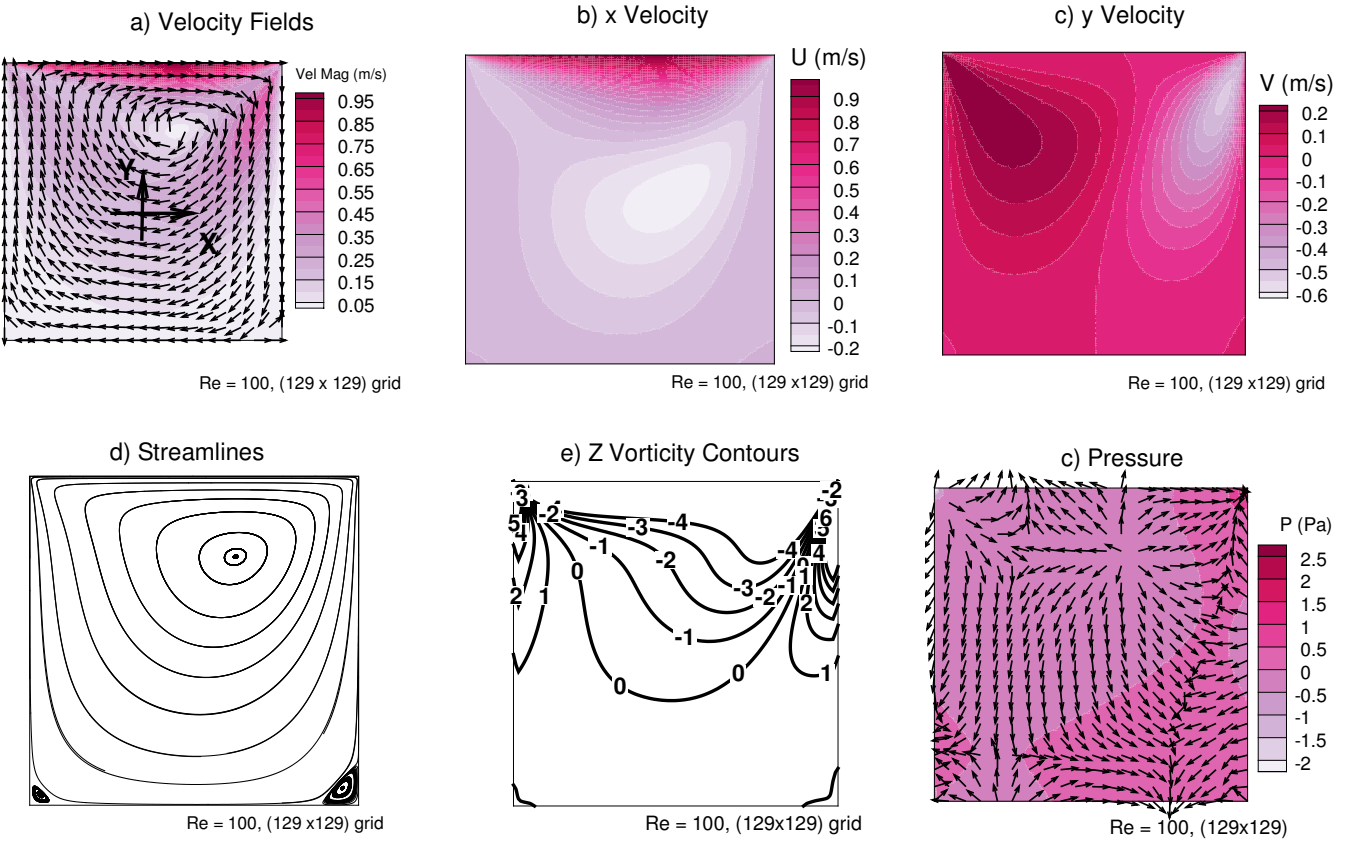


Figure 5: A unit square cavity with $Re = 100$ for a 129×129 grid. The lid moves in the positive x sense.

In figure 5 the Reynolds number is still low enough that viscous effects are assuaging the non-linear convective term. The Reynolds number is representing the relative effect of the non-linear inertial term against the resistance of viscosity, and for higher Re the inertial terms begin to dominate. $Re = 100$ is still securely within the viscous regime as commented by Burggraf. We can see the vortex core has drifted towards the downstream corner and upwards away from the cavity centre, as Burggraf observes. According to Burggraf, we should see it migrate back towards

the centre for higher Reynolds numbers. Comparison of figure 5d with figure 2a and 2b, which is between a SIMPLE implementation, a relaxation procedure in the case of Burggraf and a vorticity-streamfunction formulation with Ghia, shows good agreement. Indeed, Ghia commented in 1982 that agreement amongst researchers is good for $Re = 100$ and that only higher Reynolds numbers present more of a challenge.

Figure 5a is showing a scalar field of velocity magnitude, that is a combination of figure 5b and 5c. The vector field of velocity is also overlayed. The maximum value of the y component of velocity occurs in the negative sense at the downstream end, with strength -0.6 m/s. There is a mild rise in velocity upstream in the positive sense, with strength 0.2 m/s. This suggests a sort of looping motion between the two corners, which may develop into a feedback loop. Indeed, at much higher Reynolds number (≈ 8000) the steady condition is broken by Hopf instabilities, where a vortex street between the central vortex and boundary layers feeds itself causing oscillations in a kind of feedback loop[1]. Returning to figure 5a, fluid is pushed down strongly at the downstream edge, and pulled mildly towards the upstream corner, as also evident in figure 5c. The motion is caused by the lid which, prescribed with the no-slip condition, exerts a shear force on the adjacent fluid so that it has same velocity as the lid. Momentum is then diffused down into the cavity by viscous diffusion which is the final term in equation 23, and travels deepest into the cavity where velocity is generally lower, at the centre. There is negative horizontal velocity, u , close to the centre of the cavity and this follows naturally from the negative v component upstream, forming the arch or loop connecting the two corners in figure 5a. The flow is steady which means the time derivative in the incompressible N-S is zero or close to zero. This means snapshots of the flow at $t = 5$, $t = 120$ s, or $t = 2$ hours, for example, would theoretically show the same fields as figure 5. This is likely more true when the non-linear term is suppressed, and less so for higher Reynolds number were turbulence or instabilities might appear.

Figure 5b shows that lower down in the cavity and for the majority of the cavity the velocity is slightly negative or zero. However, at the corners there are two patches showing a change in sense of direction to a positive sense. Looking at the vertical velocity in figure 5c, the left side has slightly higher velocity generally than the right, and there is a drop in v at the corner region. Most of the downstream side has slightly negative velocity, except for the corner region where the flow direction flips. In each case for figure 5b and 5c, the flow direction flips. Analysing the vector field in figure 5a makes this even clearer, showing that the corner vortices are counter-rotating with respect to the general rotation in the rest of the cavity. With regards to the infinite series of geometrically decreasing corner vortices of Moffat, there is no evidence of a second change in direction, which is as we expect for such a low Reynolds number[14].

Referring now to our governing equation 23, the local acceleration and non-linear convective acceleration of a fluid parcel is balanced by the forces of the pressure field and viscous diffusion of momentum. This viscous diffusion term is transporting momentum to the fluid parallel to the lid, but as the pressure gradient field is showing in figure 5e, towards the corner where the pressure is high at 2.5 Pa, there is a resistance to this viscous diffusion of momentum from the pressure field. The velocity acts in an opposite sense to the direction of pressure gradient, hence $-\nabla p$ in equation 23, and the influence of the pressure field on the flow field is greater whilst the Reynolds number is lower. Indeed, at the corners there exist pressure singularities which are driving the flow from downstream to upstream in opposition to the lid-driven motion. These are a type of the classical Taylor scraping problem[15].

Figure 7d shows the streamlines. These are identical to the results of Burggraf and Ghia in figure 2a and figure 2b. The vortex core has migrated towards the downstream corner, and the downstream corner vortex is significantly larger than upstream. Analysing the vorticity contours, there are some discrepancies with the results of Ghia *et al.* in figure 2c, particularly there appears a kink in the contour along the vertical walls. In addition, Ghia observes a region of negative vorticity at the centre lower wall of the cavity.

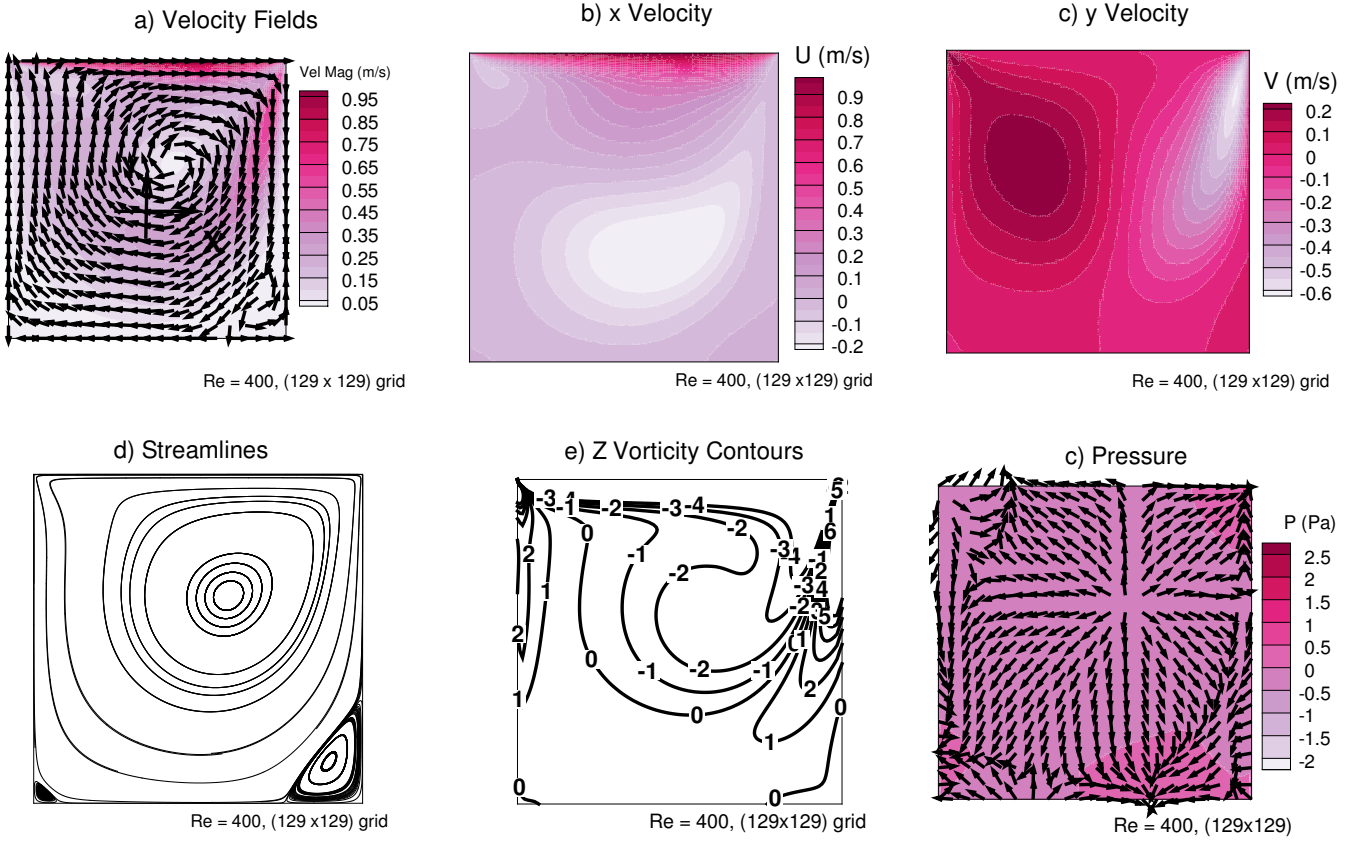


Figure 6: A unit square cavity with $Re = 400$ for a 129×129 grid. The lid moves in the positive x sense.

Comparing figure 6e and 7e for the vorticity plots with the paper of Ghia *et al.*, there is good agreement. It is unclear whether differences are from the implementation, or simply the presentation of the contours. The grids were kept identical (129×129) to facilitate comparisons.

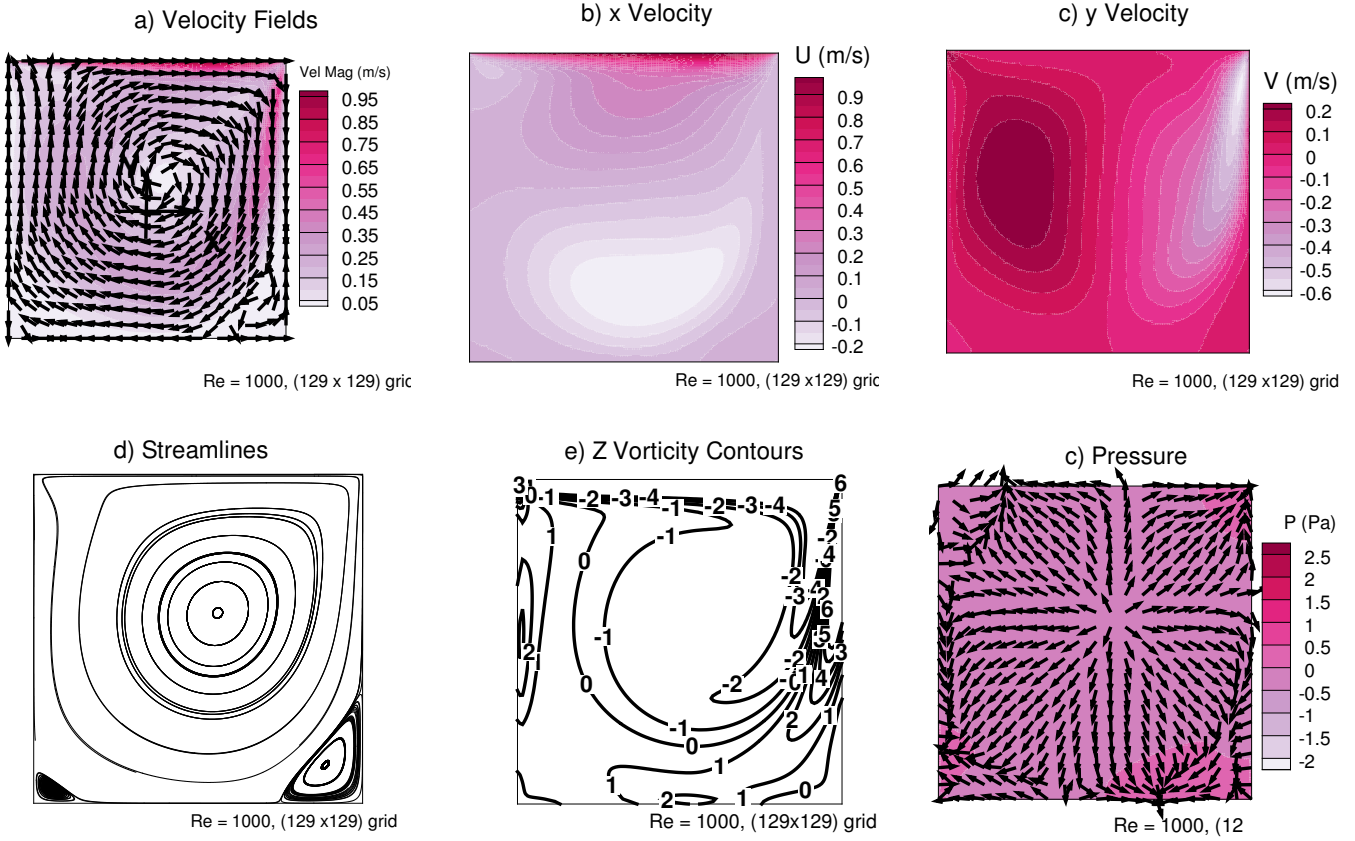


Figure 7: A unit square cavity with $Re = 1000$ for a 129×129 grid. The lid moves in the positive x sense.

Tracking figures 5d, 6d, and 7d, it is evident that as Burggraf commented the core of the recirculating eddy migrates back towards the centre of the cavity for a flow greater than $Re = 100$. This is as the inviscid core develops, and viscous effects become confined more towards the walls of the cavity. Thinking about equation 23, this may be the pressure field having less of an effect as Reynolds number increases, hence the core is not so influenced by the upstream singularity. We expect that a third eddy, which does not follow the Moffat phenomena, should appear around $Re \approx 1000$ along the upstream side wall, however this appears not to be the case.

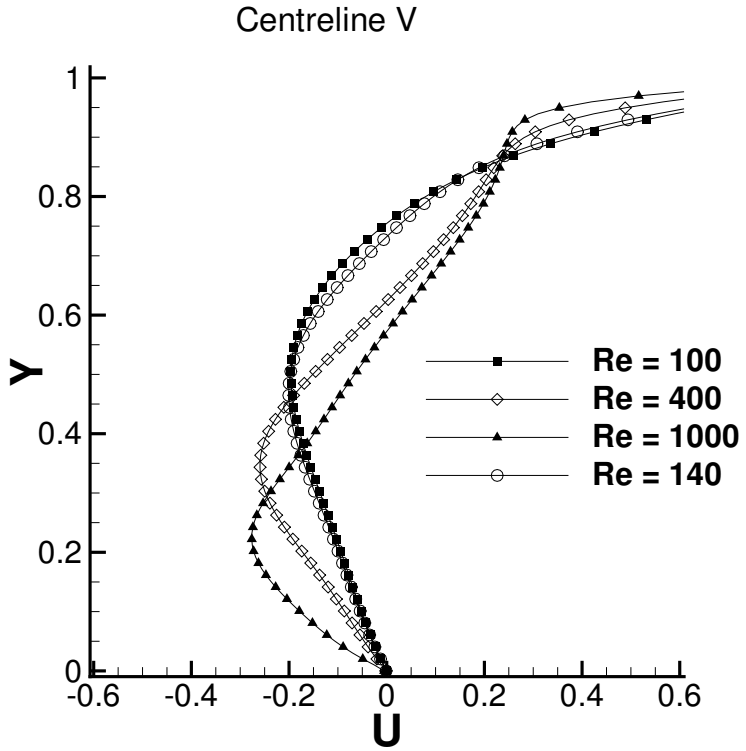


Figure 8: Centreline velocities at each Reynolds number.

Similar conclusions can be drawn from figure 8, which shows a similar trend to Ghia *et al.*, where increasing Reynolds number causes the central portion of the velocity profile to become linear. This is akin to the boundary layers becoming thinner, so viscous effects are contained more towards the surfaces of the cavity, and inertial effects begin to dominate. As the viscous layer is ‘condensed’ with growing Reynolds number the need for a finer lattice, as Burggraf commented, becomes evident. The linear profile is evidence of a vortex with an inviscid core, so a rigid body rotation, as predicted by Batchelor[7].

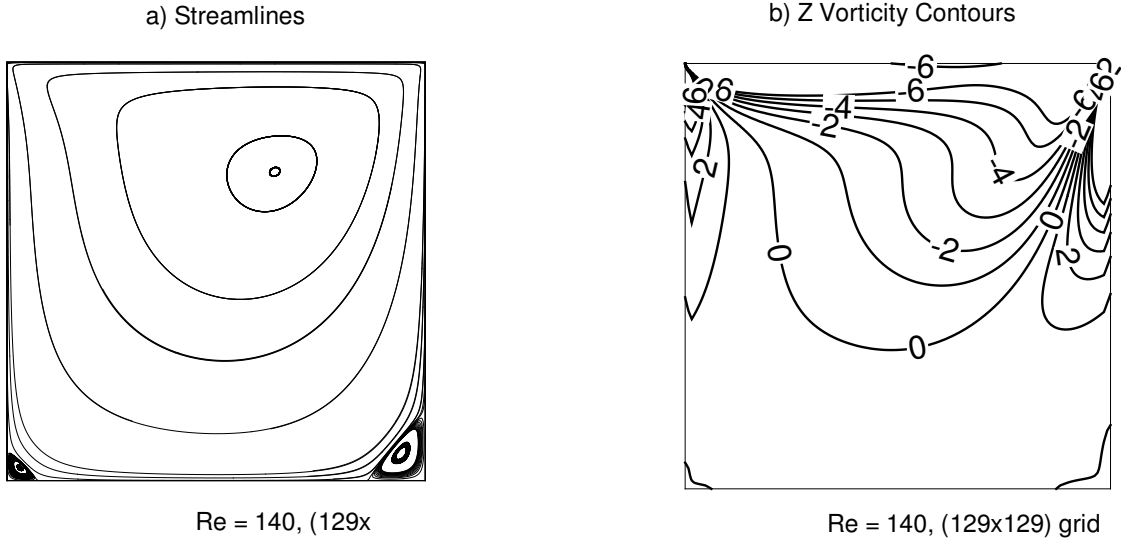


Figure 9: Personal Reynolds number, $Re = 140$, on a 129x129 grid.

5 Conclusions and Future Work

The SIMPLE method is shown to be in good agreement with the literature for low Reynolds number. At higher Reynolds number, the possibility of instabilities emerging, finer grid resolution for the viscous layers, and increased difficulty of modelling in general might make the SIMPLE method less suitable, it being more of a robust, engineering solution. More accurate alternatives should be considered for higher Reynolds numbers.

In general, inertial effects have dominated viscous effects with increasing Reynolds number, and the extent of the impact of the pressure gradient has decreased. The inviscid vortex appears and the viscous regions become contained in thin layers near the walls. The centre of the recirculating eddy returns to the cavity centre. Furthermore, the downstream corner eddy appeared larger than upstream, and no tertiary Moffat eddies appear in the corners. The upstream eddy along the vertical wall did not appear.

Future work should focus on assessing the suitability of SIMPLE for higher Reynolds numbers, or extend to more complex cases like 3-D. A proper account of the corner discontinuities should be taken. An interesting case to investigate further would be the onset of unsteadiness around $Re = 8000$ with the onset of so-called Hopf instabilities.

References

- [1] Hendrik C. Kuhlmann and Francesco Romanó. *Computational Modelling of Bifurcations and Instabilities in Fluid Dynamics*. Number volume 50 in Computational methods in applied sciences. Springer, Cham, 2019. Literaturangaben.
- [2] S. V. Patankar and D. B. Spalding. A Calculation Procedure for Heat, Mass and Momentum Transfer in Three-Dimensional Parabolic Flows. *International Journal of Heat and Mass Transfer*, 15(10):1787–1806, October 1972.
- [3] C. K. Aidun, N. G. Triantafillopoulos, and J. D. Benson. Global stability of a lid-driven cavity with throughflow: Flow visualization studies. *Physics of Fluids A: Fluid Dynamics*, 3(9):2081–2091, September 1991.
- [4] P. N. Shankar and M. D. Deshpande. Fluid Mechanics in the Driven Cavity. *Annual Review of Fluid Mechanics*, 32(1):93–136, January 2000.
- [5] Mitutosi Kawaguti. Numerical Solution of the Navier-Stokes Equations for the Flow in a Two-Dimensional Cavity. *Journal of the Physical Society of Japan*, 16(11):2307–2315, November 1961.
- [6] Odus R. Burggraf. Analytical and numerical studies of the structure of steady separated flows. *Journal of Fluid Mechanics*, 24(1):113–151, January 1966.
- [7] G. K. Batchelor. On steady laminar flow with closed streamlines at large Reynolds number. *Journal of Fluid Mechanics*, 1(2):177–190, July 1956.
- [8] U. Ghia, K. N. Ghia, and C. T. Shin. High-Re solutions for incompressible flow using the Navier-Stokes equations and a multigrid method. *Journal of Computational Physics*, 48(3):387–411, December 1982.
- [9] R. Schreiber and H. B. Keller. Driven cavity flows by efficient numerical techniques. *Journal of Computational Physics*, 49(2):310–333, February 1983.
- [10] J. R. Koseff and R. L. Street. The Lid-Driven Cavity Flow: A Synthesis of Qualitative and Quantitative Observations. *Journal of Fluids Engineering*, 106(4):390–398, December 1984.
- [11] O. Botella and R. Peyret. Benchmark spectral results on the lid-driven cavity flow. *Computers amp; Fluids*, 27(4):421–433, May 1998.
- [12] Suhas V. Patankar. *Numerical Heat Transfer and Fluid Flow*. CRC Press, Boca Raton, FL, 1980. Originally published in print: 1980.
- [13] Francis H. Harlow and J. Eddie Welch. Numerical Calculation of Time-Dependent Viscous Incompressible Flow of Fluid with Free Surface. *The Physics of Fluids*, 8(12), December 1965.
- [14] H. K. Moffatt. Viscous and resistive eddies near a sharp corner. *Journal of Fluid Mechanics*, 18(1):1–18, January 1964.
- [15] G. I. Taylor. Similarity solutions of hydrodynamic problems. *Aeronautics and Astronautics (Durand Anniversary Volume)*, pages 21–28, 1960.